Journal of GeoEngineering, Vol. 12, No. 2, pp. 65-79, June 2017
http://dx.doi.org/10.6310/jog.2017.12(2).3

CASE STUDIES FOR SIDE RESISTANCE OF BARRETTE PILES USING RESULTS OF ULTIMATE LOAD TESTS

Min-Chih Hsu [1*], Ching-Han Yu [2], and Cheng-Hsing Chen [3]

ABSTRACT

A comprehensive analysis for the side resistances of barrette piles is carried out based on five ultimate load tests on piles located in the Taipei Basin and Kaohsiung City. All piles are loaded to their ultimate conditions with pile head displacements larger than 10% of the barrette's thickness. Based on the strains measured at several depths along the pile shaft, complete side resistance *t-z* curves for various soil strata are retrieved. The characteristics of side resistances for cohesive and cohesionless soils are then quantitatively determined. Except for soil strata with gravel, most of the *t-z* curves exhibit a deflection-softening behavior. The peak resistances occur at a local pile displacement of approximately 20 mm, and the residual strength will be slightly reduced to a ratio of 0.79 ~ 0.92 at a local pile displacement of 10% of the thickness of the barrette pile. The side resistance generally increases with the effective overburden pressure. In addition, the relationship between the side resistance and the soil's SPT *N*-values, as well as the undrained shear strength, are calculated and compared with the empirical formula commonly used in engineering practice. Results show that the empirical formulae defined in the Design Specifications of Structural Foundations in Taiwan are conservative for estimating the side resistance of barrette piles.

Key words: Barrette pile, side resistance, *t-z* curve.

1. INTRODUCTION

In recent years, the use of barrette piles as the foundations of high-rise buildings has become very popular in Taiwan (Yu *et al*. 2013). The barrette pile is actually an isolated unit of the diaphragm wall, constructed using the trenching method for constructing a slurry wall. It has a slender rectangular shape resembling a wall and is therefore known as a walled-type pile. The barrette pile's considerably larger bearing capacity compared to that of the conventional circular pile is a crucial advantage in meeting the increasing demand of loading from tall buildings. In addition, the time required for trenching of barrette piles is less than that required for the drilling method employed for circular piles. Therefore, barrette piles have become increasingly common in the construction of high-rise buildings in Taiwan, especially in the Taipei and Kaohsiung areas. Barrette piles have also been used as foundations in many other countries to date. Its cross-section and construction method differ from those of conventional circular bored piles, resulting in different bearing behaviors for the two types of piles. However, no exclusive design specifications for barrette piles have been available thus far. In engineering practice in Taiwan, the bearing capacity of a barrette pile is still estimated using the same method that is used for circular piles, as defined in the design code (MOI 2001). Further studies and verifications are indeed necessary for the design of barrette piles.

For some important construction projects, *in situ* pile load tests are often conducted for verification. However, for conducting *in situ* tests on a full-scale long barrette pile, a very large compressional force is usually required to be applied at the pile head. Due to the limitation of the loading capacity of the test setup, most field tests conducted aim to merely assure a sufficient bearing capacity for design purposes and are rarely conducted to the ultimate load conditions (Chang *et al*. 2011). Therefore, it is very important and valuable to obtain results of ultimate load tests in order to characterize the side resistances and end bearing of barrette piles for engineering applications. Case studies on field test data are expected to be a valuable reference for barrette pile applications.

In this study, data of eight compressive load tests on barrette piles located in the Taipei Basin and Kaohsiung City were collected. Among them, five piles were loaded to their ultimate loading conditions. Based on the load transfer curves obtained from the tests, the side friction and end bearing of the piles were determined. The purpose of this study is to investigate the side resistance of barrette piles based on the *t-z* curves retrieved from the ultimate load tests.

2. LITERATURE REVIEW

Barrette piles have been used for many years. They are treated as rectangular piles in engineering applications. Some results of investigations of the bearing capacities of barrette piles (Tsai 2006; Chang *et al*. 2011) have shown that they are indeed larger than the bearing capacities of conventional circular bored piles. However, no specific design specifications have been made available thus far. In engineering design works, the bearing capacity of barrette piles is still estimated using the same method as that used for circular piles.

Manuscript received February 6, 2017; revised April 13, 2017; accepted April 14, 2017.
[1] Ph. D. Candidate (corresponding author) Department of Civil Engineering, National Taiwan University, Taipei, Taiwan (e-mail: hsuleonard@gmail.com).
[2] Chairman, Sino Geotechnology, Inc., Taipei, Taiwan.
[3] Emeritus Professor, Department of Civil Engineering, National Taiwan University, Taipei, Taiwan.

For conventional circular bored piles, considerable analytical and field testing data are available in the literature and many design codes or specifications have been developed and published. From a practical point of view, they form the design basis for engineering applications. The commonly used methods for estimating the side resistances of bored piles will be briefly described as below.

(1) Reese and O'Neill (1988, 1999)

Reese and O'Neill (1988) summarized non-dimensional *t-z* curves for cohesive soils based on the test results of bored piles, as shown in Fig. 1. The *t-z* curves for cohesive soils usually exhibit a deflection-softening behavior, and the peak value t_{max} develops at a rather small local pile displacement, approximately 0.6% of the pile diameter *D*.

O'Neill and Reese (1999) summarized non-dimensional *t-z* curves for cohesionless soils, as shown in Fig. 2. These curves can exhibit either deflection-softening or deflection-hardening behaviors, although, on average, the general trend approaches a deflection-softening behavior. As shown in Fig. 2, the peak side resistance is developed at a local pile displacement of 0.8 ~ 1.0% of the pile diameter, and the deformation behavior is slightly softened thereafter. As for gravel, the *t-z* curve usually exhibits a deflection-hardening behavior, and the side resistance generally increases with increasing local pile displacement.

(2) API (2002)

In the Recommended Practice of the American Petroleum Institute (API 2002), the non-dimensional *t-z* curves were published as shown in Fig. 3 for general piles (drilled and driven), especially for pile designs in offshore structures. It is suggested that the non-dimensional *t-z* curve for cohesive soils indicates a deflection-softening behavior. The peak side resistance is developed at a local pile displacement of approximately 1% of the pile diameter, and the residual strength ratio t_{res}/t_{max} is reduced to a range of 0.7 ~ 0.9. For cohesionless soils, it is suggested to simplify the *t-z* curve as a perfect elasto-plastic model. The yield local pile displacement is defined at 0.1 inch.

(3) Design Specifications of Structural Foundations in Taiwan (MOI 2001)

For practical design works in Taiwan, the empirical formula specified in the Design Specifications of Structural Foundations (MOI 2001) is commonly used. The side resistance for bored piles is estimated on the basis of the blow counts *N* of the standard penetration test (SPT) or the undrained shear strength s_u of the soils. The side resistance for cohesionless soils is estimated to be $3.3N$ kN/m^2 and that for cohesive soils is estimated to be αs_u, where α is a coefficient usually equal to 0.45 in design.

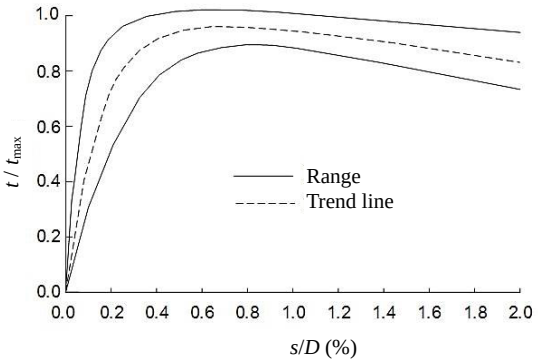

Fig. 1 Normalized *t-z* curves in cohesive soil (Reese and O'Neill 1988)

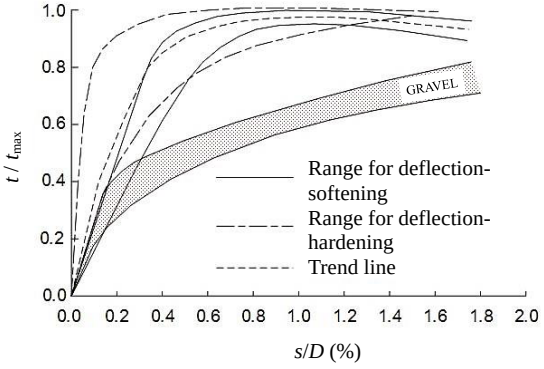

Fig. 2 Normalized *t-z* curves in cohesionless soil (O'Neill and Reese 1999)

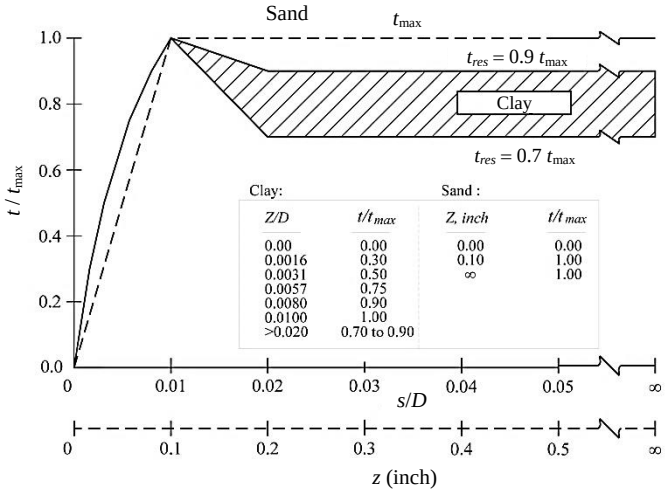

Fig. 3 Typical *t-z* curves (API 2002)

3. LOAD TESTS ON PILES AT THE TAIPEI SITE

3.1 Test Program and Site Conditions

A total of six pile load tests were selected for investigation, designated as TP1 ~ TP6 in Fig. 4. The test sites were located in a newly developed residential area near Xindian Creek, which runs through the southern part of the Taipei Basin. The shaded blocks shown in Fig. 4 have been thoroughly investigated by hundreds of exploration borings. The six boring logs drilled at the locations of the pile load tests are shown in Fig. 5. The groundwater level is located at a depth of 5 ~ 6 m below the ground surface. Based on the results of explorations and laboratory testing, the geological setting of this area can be divided into several sublayers (Fig. 5):

(1) Sublayer I: Backfill material and silty clay (SF/CL)

From the ground surface to a depth of approximately 10 m, the first layer is classified as SF/CL, a layer of backfill materials overlying a layer of soft-to-medium stiff silty clay of varying thickness.

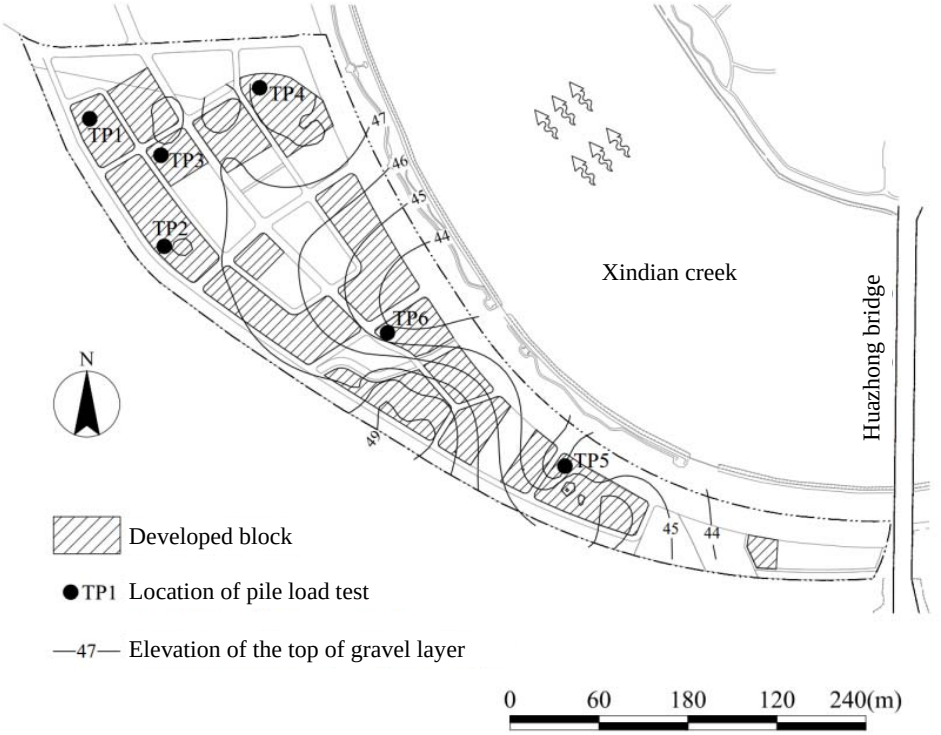

Fig. 4 Site plan and locations of test barrette piles (Taipei site)

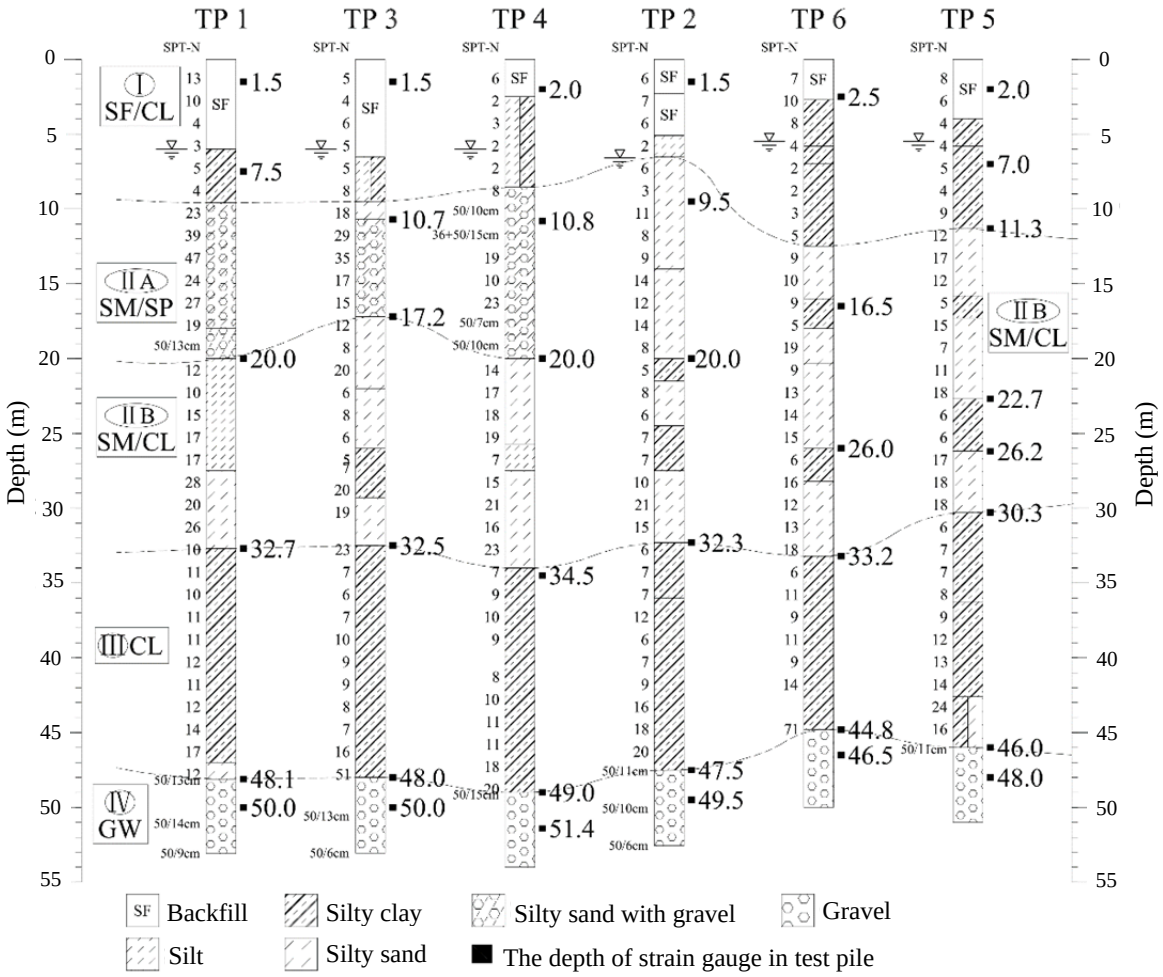

Fig. 5 Boring logs at the location of test barrette pile and depths of strain gauge installed (Taipei site)

(2) Sublayer II: Silty sand (SM/SP, SM/CL)

The second sublayer is a layer of silty sand around 20 m thick, with some interlayers of gravelly soil or clay. In the northern part of the study area (drilling holes TP1, TP3, and TP4), the silty sand contains some gravelly soil at a depth of 10 ~ 20 m and is classified as Sublayer IIA (SM/SP). Underneath is a layer of silty sand with some clay and it is classified as Sublayer IIB (SM/CL).

In the southern part of the study area (drilling holes TP2, TP5, and TP6), the soil distributed at a depth of 10 ~ 32 m is mainly medium dense silty sand with some silty clay. It is classified as Sublayer IIB (SM/CL).

(3) Sublayer III: Silty clay (CL)

At a depth of 32 ~ 45 m, there exists a thick layer of medium stiff to stiff silty clay, stratified with thin layers of clayey silt.

(4) Sublayer IV: Gravel (GW)

At a depth of approximately 45 m below the ground surface, a thick gravel layer known as the Chingmei Formation can be found. The major content of this layer is cobble and gravel with fine-to-coarse silty sand. All SPTs conducted showed that the *N*-values are all much larger than 50. This layer is usually adopted as the supporting layer of pile foundations for construction works in the Taipei Basin area.

The test barrette piles TP1 ~ TP6 have a nominal size of 0.8 m × 2.6 m in cross-section and a penetration depth of 3 m into the gravel formation (Table 1). They were constructed using the slurry method using a MASAGO hydraulic long bucket and the polymer slurry as the stabilizing fluid during the trench excavation. Considering that soft materials and debris may remain at the bottom of the pile, base grouting was applied for piles TP1 ~ TP4, while piles TP5 and TP6 were not base grouted for comparison purposes. The axial compression load test followed the quick test procedure specified in the ASTM D1143/D1143M-07.

3.2 Results of Pile Load Tests

Load-Displacement Curves at the Pile Head

The results of the six load tests are summarized in Table 1, and the relationships between load and displacement recorded at the pile head are plotted in Fig. 6. Based on this figure, it can be seen that the tests on TP1 ~ TP3 were not conducted at their ultimate conditions, as the tests were terminated at rather smaller pile head displacements. The TP1 test was terminated at a load of 36 MN because concrete breakage unexpectedly occurred near the pile head; the pile head displacement recorded was merely 41 mm.

The tests on TP4 ~ TP6 were conducted to have respective maximum loads of 70 MN, 40 MN, and 36 MN, and reached respectively maximum pile head displacements of 177 mm, 151 mm, and 161 mm, which are considerably larger than 10% of the barrette pile thickness. These three tests can be regarded as having reached their ultimate loading conditions. It should be noted that pile TP4 was base grouted, while piles TP5 and TP6 were not. Therefore, the ultimate test load for TP4 was much larger than those of TP5 and TP6, that is, approximately double. Base grouting clearly had a significant effect on the ultimate bearing capacity of the piles.

Skin Friction and End Bearing

In the literature, the skin friction and end bearing of circular piles are commonly represented by nonlinear *t*-*z* and *q*-*w* curves, respectively, deduced from the results of pile load tests (Coyle and Reese 1966; Reese *et al*. 2006). Although a barrette pile has a slender rectangular shape, quite different from a circular pile, the same technique that is used for circular piles is used in this study to obtain the *t*-*z* and *q*-*w* curves in order to represent the skin friction and end bearing of a barrette pile (Ng *et al*. 2000, 2003; Ho and Lim 1998).

For the barrette piles investigated in this study, a series of strain gauges were installed at various depths of the steel cage (six gauges per level; Fig. 5). The strain gauges were installed at the depths of the interfaces between soil stratifications, marked with black squares in Fig. 5. The strains measured during the load tests can be used to obtain the load transfer curve along the pile shaft, as well as the vertical displacement at each strain gauge location. Based on the soil strata defined in Section 3.1, the *t*-*z* curves deduced for each soil stratum for the six pile tests are shown in Fig. 7, and the *q*-*w* curves deduced for the gravel sublayer for piles TP1 ~ TP5 are shown in Fig. 8. The *t*-*z* curves for Sublayer I are not included in Fig. 7 because of the large variations among the piles, possibly resulting from the non-uniform backfill materials and the trench protection works (guide walls) remaining near the ground surface.

Table 1 Summary of test barrette pile geometry and load test results

Site	Pile load test designation	Nominal dimension ($B \times L$, m)	Pile length (m)	Socket length in gravel formation (m)	Base grouting	Maximum test load (MN)	Total displ. at max. test load (mm)
Taipei	TP1	0.8 × 2.6	50.5	3	Grouted	36	41
	TP2	0.8 × 2.6	50.5	3	Grouted	42.2	30
	TP3	0.8 × 2.6	51.0	3	Grouted	45	35
	TP4	0.8 × 2.6	52.0	3	Grouted	70	177
	TP5	0.8 × 2.6	49.0	3	Ungrouted	40	151
	TP6	0.8 × 2.6	47.8	3	Ungrouted	36	161
Kaohsiung	KP1	1.0 × 2.6	75.0	–	Ungrouted	55	126
	KP2	1.0 × 2.6	75.0	–	Ungrouted	57	121

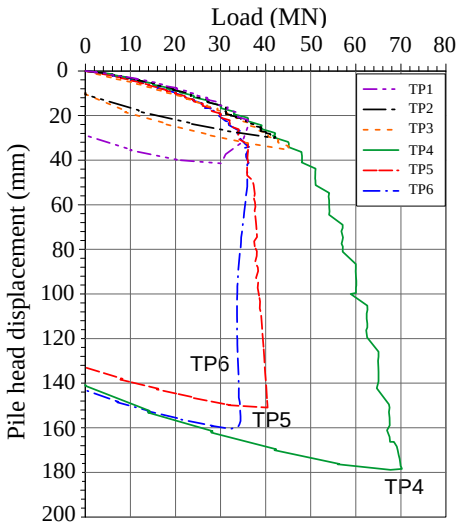

Fig. 6 Load-displacement curves at pile head (Taipei site)

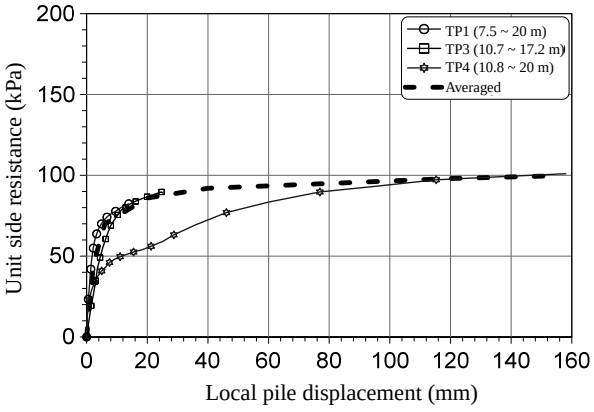

(a) Silty sands with some gravel (sublayer IIA, SM/SP)

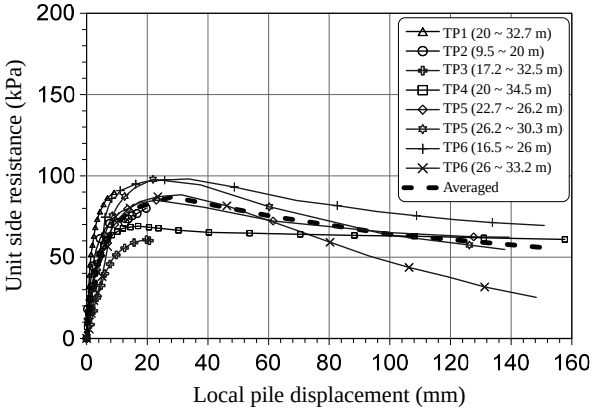

(b) Silty sands with some clay (sublayer IIB, SM/CL)

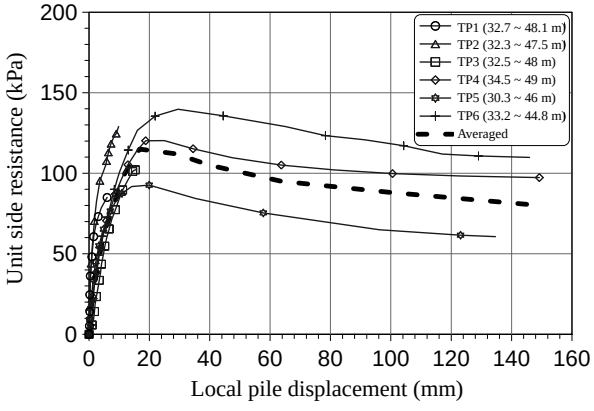

(c) Silty clays (sublayer III, CL)

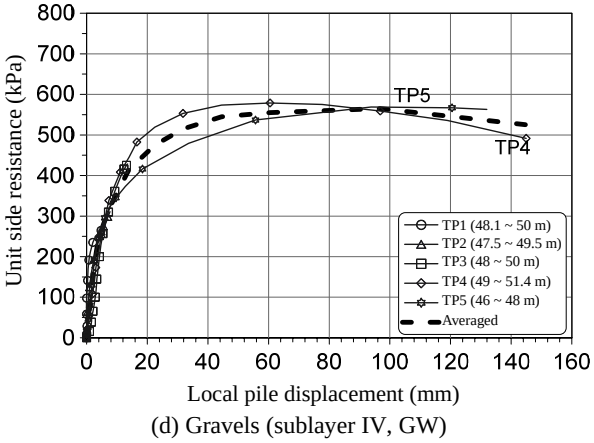

(d) Gravels (sublayer IV, GW)

Fig. 7 *t-z* curves for each soil stratum (Taipei site)

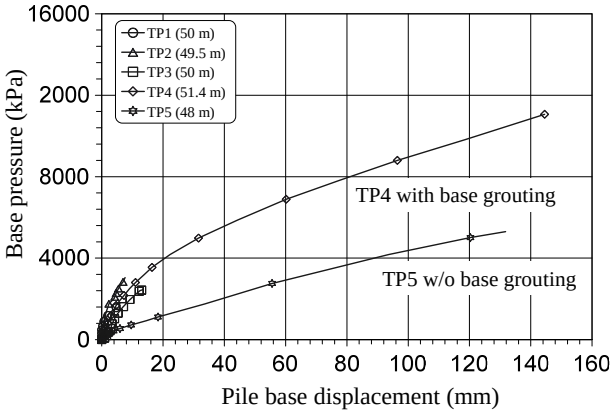

Fig. 8 *q-w* curves at barrette base (Taipei site)

The *t-z* curves for the layers of silty sand with some clay (sublayer IIB, Fig. 7(b)) and with silty clay (sublayer III, Fig. 7(c)) exhibit a slight deflection-softening behavior after the peak side resistance is reached, which appears to be mobilized at a local pile displacement of approximately 20 mm.

For the layer of silty sand with some gravel (sublayer IIA, Fig. 7(a)) and for gravel layer (sublayer IV, Fig. 7(d)), the *t-z* curves show a slight deflection-hardening behavior. The ultimate unit side resistance of the gravel layer appears to be mobilized beyond a displacement greater than 40 ~ 60 mm; this observation is similar to other pile load test results of gravel formation in the Taipei area (Yu 2015). This can likely be attributed to the irregularities or roughness of the pile-soil interface and the tendency of gravel to dilate during shearing.

The *q-w* curves for piles TP1 ~ TP5 were determined from the measurement data obtained from the strain gauges installed at the lowest level of each pile, about 1 m above the pile toe (Fig. 8). Because the lowest strain gauges in TP6 malfunctioned before the test, the *q-w* curve could not be retrieved for this pile. The *q-w* curves for TP4 and TP5 exhibit an initial curved section followed by an approximately straight line under larger pile base displacement. This indicates the absence of a failure mode at the pile toe due to an increase in the base resistance with increasing pile base displacement.

3.3 Back Analyses

The appropriateness of the *t-z* and *q-w* curves obtained in the previous section can be verified through back analyses. Back analyses were performed for piles TP4 and TP5, which had reached the ultimate loading conditions during the tests.

The nonlinear *t-z* and *q-w* curves for each soil stratum are shown in Figs. 7 and 8. For each group, an approximate average line is drawn to represent the characteristic relationship for each sublayer. The approximate averaged curves together with the deduced *t-z* curve of Sublayer I (SF/CL) and the *q-w* curve of TP4 were employed to conduct back analyses on the TP4 load test. In addition, the approximate averaged curves together with the deduced *t-z* curve of Sublayer I (SF/CL) and the *q-w* curve of TP5 were employed to conduct back analyses on the TP5 load test. The dashed lines in Fig. 9 represent the respective back analysis responses. The back-calculated results for both cases closely match the field test results. It can be concluded that the nonlinear *t-z* and *q-w* curves retrieved from the load tests can appropriately represent the characteristics of soil strata at the study site.

4. LOAD TESTS ON PILES AT THE KAOHSIUNG SITE

4. 1 Test Program and Site Conditions

Two pile load tests, designated as KP1 and KP2, were selected for our case studies. The piles were located in an alluvial deposit near the Kaohsiung Harbor (Fig. 10). The two boring logs drilled at the locations of the pile load tests are shown in Fig. 11. The subsoil of this area primarily consists of sand and sandy silt, with interlayers of clay. The groundwater level is located at a depth of 4 ~ 5 m below the ground surface. Based on the results of explorations and laboratory tests, the geological setting of this area can be divided into the following sublayers (Fig. 11):

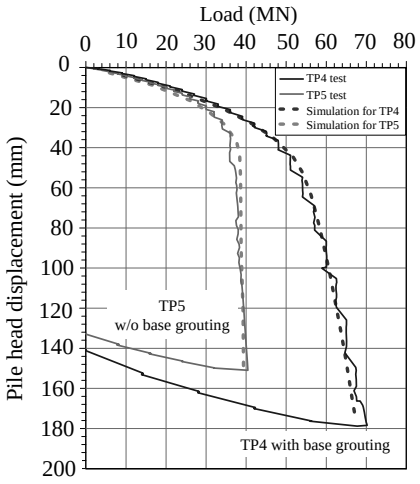

Fig. 9 Back-calculated and measured load-displacement curves (Taipei site)

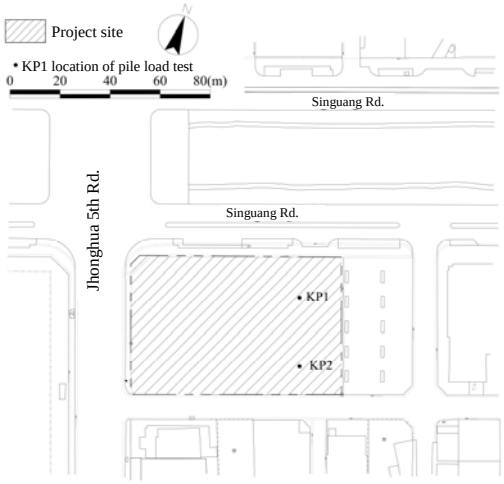

Fig. 10 Site plan and locations of test barrette piles (Kaohsiung site)

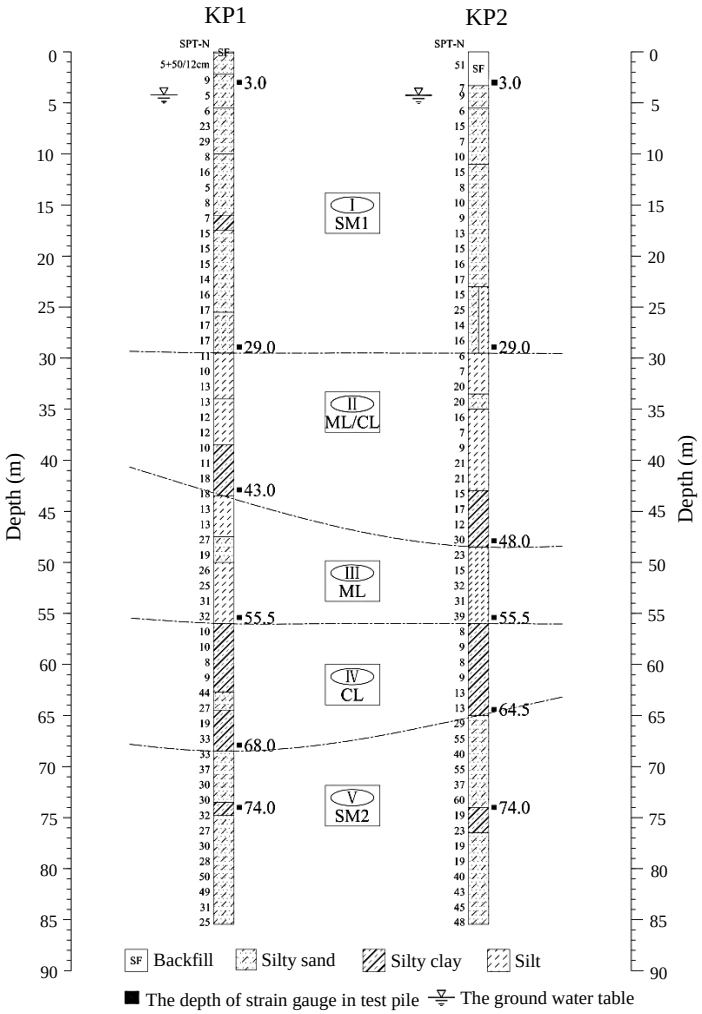

Fig. 11 Boring logs at the location of test barrette pile and depths of strain gauge installed (Kaohsiung site)

(1) Sublayer I: Silty Sand (SM1)

From the ground surface to a depth of approximately 29 m, the first layer is classified as loose to medium-dense silty sand, except some backfill materials existing near the ground surface. The SPT *N*-values range from 5 to 29.

(2) Sublayer II: Nonplastic silt with clay (ML/CL)

The second sublayer is a 14 ~ 19-m-thick layer of sandy silt, with some interlayers of clay. The SPT *N*-values range from 6 to 30.

(3) Sublayer III: Nonplastic silt (ML)

This layer consists of nonplastic silt of varying thicknesses of 7.5 ~ 12.5 m, with some thin interlayers of silty sand. The SPT *N*-values range from 13 to 39.

(4) Sublayer IV: Silty clay (CL)

At a depth of 55.5 m to 64.5 m or 68 m, there exists a layer of medium-to stiff clay. The SPT *N*-values range from 8 to 33.

(5) Sublayer V: Silty Sand (SM2)

At a depth of approximately 64.5 m or 68 m below the ground surface, the soils are classified as dense silty sand, with SPT *N*-values ranging from 25 to 60.

Two barrette piles KP1 and KP2 were subjected to axial compression tests at this site (Table 1). Both piles had a nominal size of 1.0 m × 2.6 m in cross-section and were constructed using the slurry method as for the Taipei cases described in the previous section. No base grouting was applied for both piles.

The procedure for the axial compression load test followed the quick test procedure specified in ASTM D1143/D1143M-07. Both piles were fully instrumented with rebar strain gauges arranged at the depths of the interfaces between soil stratifications; these are marked in black squares in Fig. 11. During the test, the load transfer along the pile shaft can be completely recorded.

4.2 Results of Pile Load Test

Load-Displacement Curve at the Pile Head

The results of the two load tests are summarized in Table 1, and the relationships between load and displacement recorded at the pile head are plotted in Fig. 12. Based on this figure, it can be seen that both piles were loaded to their ultimate conditions because the pile head displacements reached 126 mm and 121 mm, respectively, which are larger than 10% of the barrette pile thickness. Both KP1 and KP2 appeared to show a slight deflection-softening behavior.

Skin Friction and End Bearing

The *t*-*z* and *q*-*w* curves determined from the KP1 and KP2 pile tests by applying the same technique used in the previous Taipei cases, based on the soil strata defined in Fig. 11, are shown in Fig. 13. All the *t*-*z* curves of sublayers I to V (Figs. 13(a) ~ 13(e)) exhibit a slight deflection-softening behavior after the peak side resistance is reached. Except for sublayer I, the peak side resistances for all sublayers appear to be mobilized at a local pile displacement of approximately 20 mm. In addition, Fig. 13 clearly shows that the side resistance for each sublayer increases with depth, *i.e.*, increases with the effective overburden pressure.

The *q*-*w* curves for piles KP1 and KP2 were determined from the data measured using the strain gauges installed at the lowest level of each pile, approximately 1 m above the pile toe. The deduced *q*-*w* curves shown in Fig. 13(f) exhibit a deflection-hardening behavior. However, it should be noted that the end bearings were developed very slowly with respect to the displacement at the toe. The mobilized bearing pressure was only 1,000 kPa at a pile base displacement of 10 mm. This indicates that the base resistance, even at a depth of 74 m below the ground surface, will not be mobilized effectively with small displacements at the toe; this aspect should be taken into consideration in engineering design.

4.3 Back Analyses

Back analysis will be performed for the Kaohsiung case using the same technique used for the Taipei case. The nonlinear *t*-*z* and *q*-*w* curves shown in Fig. 13 are used for back analysis on piles KP1 and KP2. Similarly, an approximate average line was drawn to represent the characteristic relationship for each sublayer in Fig. 13. The approximate averaged curves were employed to conduct back analyses on the KP1 and KP2 load tests. The dashed lines in Fig. 14 represent the respective back analysis responses. The back-calculated results for both cases closely match those of the field tests. It can be concluded that the nonlinear *t*-*z* and *q*-*w* curves obtained from the load tests can appropriately represent the characteristics of soil strata at the study site.

5. SIDE RESISTANCE

Among the barrette pile load tests investigated above, a total of five tests reached the ultimate conditions, *i.e.*, the TP4, TP5, and TP6 piles in the Taipei case and the KP1 and KP2 piles in the Kaohsiung case. From each test, the complete *t*-*z* curves for various soil strata have been retrieved and can be used to investigate the characteristics of side resistance on the barrette piles.

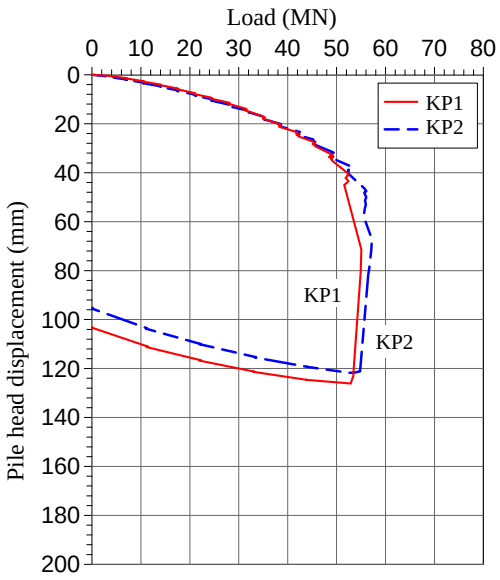

Fig. 12 Load-displacement curves at pile head (Kaohsiung site)

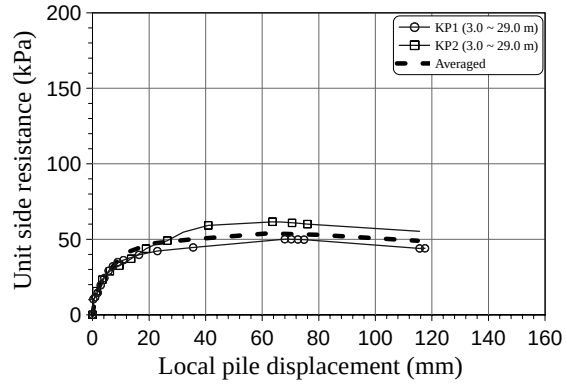

(a) *t-z* curves for silty sands (sublayer I, SM1)

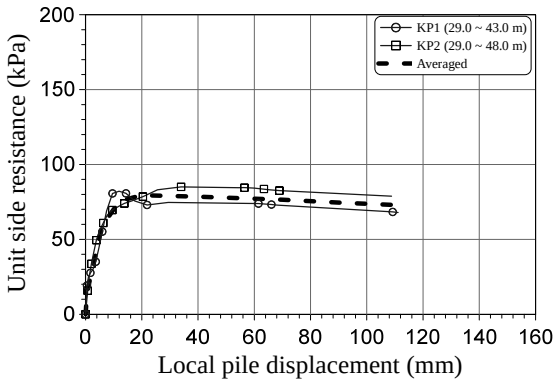

(b) *t-z* curves for nonplastic silts with clays (sublayer II, ML/CL)

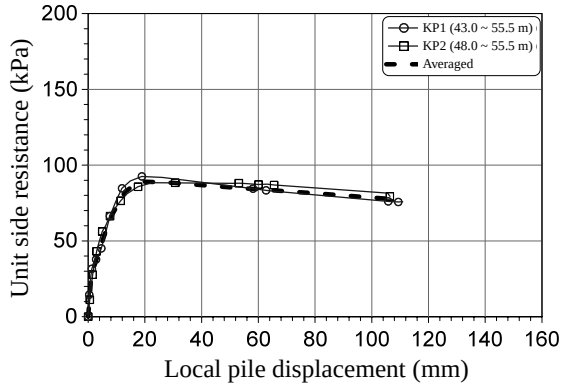

(c) *t-z* curves for nonplastic silts (sublayer III, ML)

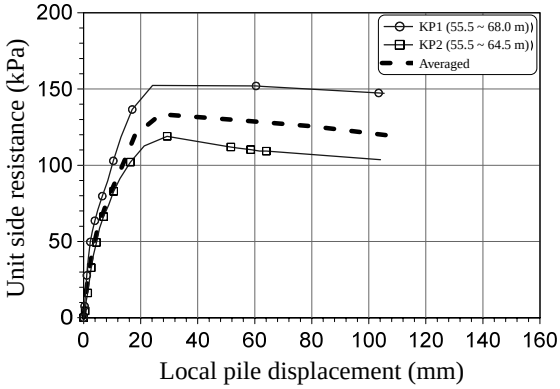

(d) *t-z* curves for silty clays (sublayer IV, CL)

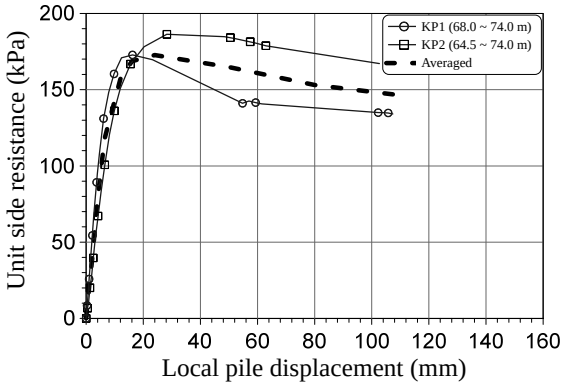

(e) *t-z* curves for silty sands (sublayer V, SM2)

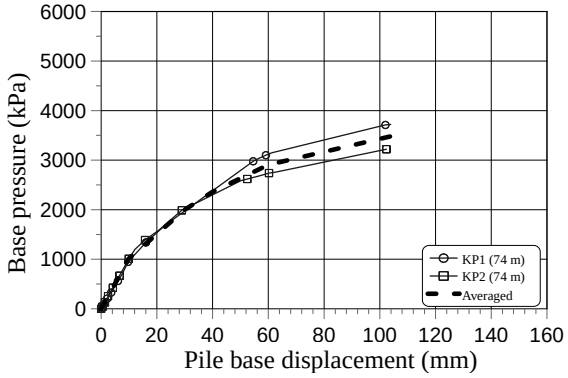

(f) *q-w* curves at barrette base

Fig. 13 *t-z* curves for each soil stratum and *q-w* curves at barrette base (Kaohsiung site)

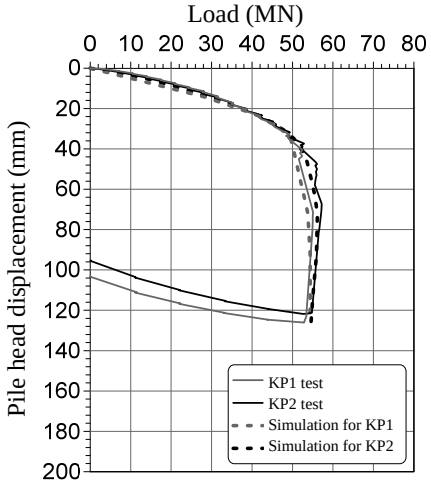

Fig. 14 Back-calculated and measured load-displacement curves (Kaohsiung site)

The side resistances are estimated based on the *t-z* curves obtained in the previous two sections and summarized in Table 2. In this table, t_{max} and z_p indicate the maximum side resistance and associated local pile displacement, while t_{res} indicates the residual side resistance considered to occur at a local pile displacement of 0.1*B* (*B* is the thickness of the barrette pile). In other words, the resistances that occurred at a local pile displacement of 80 mm for the Taipei case and 100 mm for the Kaohsiung case are taken as the residual side resistances in this study.

The side resistances tabulated in Table 2 are grouped into five categories, as discussed below.

(1) Cohesive soils in the Taipei case

For the Taipei case, in addition to Sublayer III (CL), the soils at a depth of 22.7 ~ 26.2 m in Sublayer IIB at the location of TP5 (see Fig. 5) are also characterized as cohesive soils. From the *t-z* curves, the maximum side resistance t_{max} is in the range 85 ~ 140 kPa (average 110 kPa), and occurs at a local pile displacement of 19.9 ~ 29.5 mm (average 24 mm, approximately 0.03*B*).

The associated *t-z* curves are divided by t_{max} to obtain the normalized *t-z* curves, as shown in Fig. 15(a). It can be seen that the normalized *t-z* curves exhibit softening behavior, with t_{res}/t_{max} ranging over 0.74 ~ 0.88 (average 0.82). The averaged curve of cohesive soils deduced by Reese and O'Neill (1988), shown in Fig. 1, is obtained for circular piles and plotted with respect to the dimensionless local pile displacement *s*/*D* (where *D* is the pile diameter). For the purpose of comparison, we chose the most commonly used pile of diameter D = 1.5 m and re-plotted using the dashed line in Fig. 15(a). It can be seen that Reese and O'Neill's curve has a larger initial stiffness and the peak occurs at a very small local pile displacement of approximately 9 mm (0.006*D*). After the peak, the curve drops quickly to approximately 0.80 at a local pile displacement of 30 mm (0.02*D*). Compared with this, the curves obtained from the Taipei cases show very different deformation behaviors. The initial stiffness is developed much slower and the peak occurs at a considerably larger local pile displacement of approximately 24 mm. After the peak value, the rate of stiffness reduction is extremely low, and the residual strength is retained with a ratio of 0.82 at a local pile displacement of 80 mm. It can be concluded that the softening behavior of Taipei's cohesive soils is more ductile than that shown by the trend line published by Reese and O'Neill (1988).

(2) Cohesionless soils in the Taipei case (not including the gravel formation)

For the Taipei case, the soils in Sublayer IIB, except those at a depth of 22.7 ~ 26.2 m at the location of TP5, are categorized as cohesionless soils herein. From the *t-z* curves, the maximum side resistance t_{max} is in the range 69 ~ 98 kPa (average 88 kPa) and occurs at a local pile displacement of 17 ~ 33.6 mm (average 26 mm, approximately 0.03*B*).

Similarly, the associated *t-z* curves are divided by t_{max} to obtain the normalized *t-z* curves as shown in Fig. 15(b). It can be seen that the normalized *t-z* curves exhibit a softening behavior, with t_{res}/t_{max} ranging over 0.67 ~ 0.91 (average 0.79). The averaged curve of cohesionless soils in Fig. 2, deduced by O'Neill and Reese (1999), is multiplied with a pile diameter of D = 1.5 m and re-plotted in Fig. 15(b) for comparison. It can be seen that the O'Neill and Reese's trend line is located at the upper bound of the *t-z* curves obtained in this study. That is, the Taipei cohesionless soils will have slightly smaller initial stiffness and the peak will occur at a larger local pile displacement of approximately 26 mm. This may be because the Taipei cohesionless soils are recognized to have large contents of silts.

Table 2 Corresponding characteristics of side resistance

Site	Soil type	Sublayer	Pile No. (depth, m)	t_{max} (kPa)	z_p (mm)	t_{res}@0.1*B* (kPa)	t_{res} / t_{max}	z_p / *B*
Taipei	Cohesive	III. CL	TP4 (34.5 ~ 49.0)	120	24.9	102	0.85	0.031
		III. CL	TP5 (30.3 ~ 46.0)	93	19.9	69	0.74	0.025
		III. CL	TP6 (33.2 ~ 44.8)	140	29.5	123	0.88	0.037
		IIB. SM/CL	TP5 (22.7 ~ 26.2)	85	23.0	70	0.82	0.029
	Cohesionless	IIB. SM/CL	TP4 (20.0 ~ 34.5)	69	17.0	63	0.91	0.021
		IIB. SM/CL	TP5 (26.2 ~ 30.3)	98	21.9	72	0.73	0.027
		IIB. SM/CL	TP6 (16.5 ~ 26.0)	98	33.6	82	0.84	0.042
		IIB. SM/CL	TP6 (26.0 ~ 33.2)	88	31.2	59	0.67	0.039
	Gravel	IV. GW	TP4 (49.0 ~ 51.4)	579	60.5	570	0.98	0.076
		IV. GW	TP5 (46.0 ~ 48.0)	569	93.8	–	–	0.117
Kaohsiung	Cohesive	IV. CL	KP1 (55.5 ~ 68.0)	152	21.0	148	0.97	0.021
		IV. CL	KP2 (55.5 ~ 64.5)	119	29.3	104	0.87	0.029
	Cohesionless	I. SM1	KP1 (3.0 ~ 29.0)	50	68.0	46	0.92	0.068
		I. SM1	KP2 (3.0 ~ 29.0)	62	63.6	57	0.92	0.064
		II. ML/CL	KP1 (29.0 ~ 43.0)	82	11.9	69	0.84	0.012
		II. ML/CL	KP2 (29.0 ~ 48.0)	85	34.0	80	0.94	0.034
		III. ML	KP1 (43.0 ~ 55.5)	93	18.9	77	0.83	0.019
		III. ML	KP2 (48.0 ~ 55.5)	88	22.5	82	0.93	0.023
		V. SM2	KP1 (68.0 ~ 74.0)	173	16.2	136	0.79	0.016
		V. SM2	KP2 (64.5 ~ 74.0)	186	28.2	168	0.90	0.028

(3) Chingmei gravel in the Taipei case

The maximum side resistances of piles TP4 and TP5 in the Chingmei gravel formation are determined to be 579 kPa and 569 kPa, respectively, and they occur at a local pile displacement of 60.5 mm and 93.8 mm, respectively. The normalized *t*-*z* curves are shown in Fig. 15(c). The *t*-*z* curve of TP5 shows a deflection-hardening behavior, while that of TP4 shows almost no deflection-softening with $t_{res}/t_{max} = 0.98$. For practical application purposes, the averaged curve of these two piles in the Chingmei gravel formation can be regarded as showing a hardening behavior.

The averaged curve of gravel soils in Fig. 2, deduced by O'Neill and Reese (1999), is also multiplied by a pile diameter of $D = 1.5$ m and re-plotted in Fig. 15(c) for comparison. Although O'Neill and Reese's curve is only valid to a local pile displacement of up to 25 mm (0.017*D*), it is quite consistent with the initial part of the curves obtained in this study.

(4) Cohesive soils in the Kaohsiung case

For the Kaohsiung case, only Sublayer IV (CL) at a depth of 55.5 ~ 68.0 m can be characterized as cohesive soil. From the *t*-*z* curves, the maximum side resistances for KP1 and KP2 are 152 kPa and 119 kPa, respectively, and they occur at a local pile displacement of 21 mm and 29.3 mm, respectively, *i.e.*, approximately 0.025*B*.

The *t*-*z* curves normalized by t_{max} are shown in Fig. 15(d). They show a slight softening behavior. Similarly, the average curve of cohesive soils deduced by Reese and O'Neill (1988) is multiplied by a pile diameter of $D = 1.5$ m and re-plotted in Fig. 15(d) for comparison. Although only two curves are obtained for the Kaohsiung case, the comparison gives the same conclusion as that for cohesive soils in the Taipei case. The curves obtained for the Kaohsiung case show smaller initial stiffness, and the peaks occur at a much larger local pile displacement of approximately 25 mm. After its peak value is reached, the rate of stiffness reduction is also extremely low; the residual strength is retained with a ratio of 0.92 at a local pile displacement of 100 mm. It can be concluded that the softening behavior of the Kaohsiung cohesive soils is more ductile than the average curve published by Reese and O'Neill (1988).

(5) Cohesionless soils in the Kaohsiung case

For the Kaohsiung case, all sublayers except sublayer IV (CL) are characterized as cohesionless soils. As can be seen in Table 2, the maximum side resistance of each sublayer increases with depth, from 50 kPa at a shallow depth to 186 kPa at a depth of 74 m. The effect of the effective overburden pressure is significant. Except for sublayer I, the maximum side resistances for all sublayers occur at a local pile displacement of 11.9 ~ 34 mm (0.02*B* approximately).

The *t*-*z* curves normalized by t_{max} are shown in Fig. 15(e). They show a deflection-softening behavior, with t_{res}/t_{max} ranging over 0.79 ~ 0.94 (average 0.88). Similarly, a comparison with the trend line published by O'Neill and Reese (1999) in Fig. 15(e) is made. Since O'Neill and Reese's curve is only valid to a local pile displacement of up to 25 mm, the comparison can be made only for a small local pile displacement range. O'Neill and Reese's curve shows a slightly larger initial stiffness than the curves of the cohesionless soils in the Kaohsiung case. For larger local pile displacements, the curves of the Kaohsiung case show a gentle deflection-softening behavior, yet have a residual strength ratio t_{res}/t_{max} of 0.79 ~ 0.94 at a local pile displacement of 100 mm.

6. CORRELATION STUDIES

During the design stage, it is necessary to estimate the bearing capacity of a pile that is to be constructed at a site. Although theoretical calculations based on the *c*-ϕ properties of the soil can be used, empirical formula based on the SPT *N*-values and the undrained shear strength are more often adopted in engineering practice. In Taiwan, the empirical formula used for conventional circular bored piles, specified in the Design Specifications of Structural Foundations (MOI 2001), is commonly applied. The side resistance for cohesionless soil is estimated to be $3.3N$ kN/m^2, where *N* is the blow count of the SPT. The side resistance for cohesive soil is estimated to be αs_u, where s_u is the undrained shear strength and α is a coefficient that usually takes a value of 0.45 in design.

For the case studies conducted herein, the SPT *N*-values, as well as the undrained shear strength of the soils at the locations of the load-tested piles are available. Therefore, the correlations of side resistances with the associated soil parameters can be calculated to investigate the suitability of the above-mentioned empirical formula.

6.1 Correlation of Side Resistance with SPT *N*-Values of Soils

The SPT *N*-values for each test pile in the Taipei Basin and in Kaohsiung City investigated in this study are listed in the associated boring logs shown in Figs. 5 and 11. Since the *t*-*z* curves for the test piles are deduced from values averaged over the thickness of the associated soil strata, the average *N*-value for each soil strata, termed $\overline{N}$, is accordingly calculated as shown in Table 3. Referring to the side resistances listed in Table 2, the ratios $t_{max}/\overline{N}$ and $t_{res}/\overline{N}$ are calculated as shown in Table 3.

For the cohesionless soils in both Taipei and Kaohsiung cases, $t_{max}/\overline{N}$ and $t_{res}/\overline{N}$ are plotted as shown in Figs. 16(a) and 16(b), respectively. It can be seen that the peak resistances are distributed within a small range of approximately 5*N*, while the residual side resistances are all larger than 3.4, except one point which is 2.9. Although the data points obtained in this study are limited to the sites investigated herein, the results are still very valuable for verifying the empirical equation in the Design Specifications applied in engineering practices. It can be said that the empirical formula $3.3N$ is slightly too conservative to be used to estimate the peak side resistance of barrette piles, while it is conservative and appropriate for estimating the residual side resistance of barrette piles.

For the cohesive soils of both the Taipei and Kaohsiung cases, $t_{max}/\overline{N}$ (kPa) and $t_{res}/\overline{N}$ (kPa) are plotted in Figs. 17(a) and 17(b), respectively. It can be seen that the peak resistances are distributed around the line of $10N$ kPa, while the residual side resistances are slightly smaller and distributed around the line of $9N$ kPa. In Japanese codes (JRA 2012; RTRI 1997), an empirical formula of $10N$ kPa is used to estimate the side resistance of cohesive soils. The data shown in Figs. 17(a) and 17(b) are few in number, but they are still valuable for verifying that the empirical formula of $10N$ kPa can be appropriately used for barrette piles on cohesive soils. Although this empirical

formula is appropriate for estimating the peak side resistance, it slightly over-estimates the residual side resistance.

6.2 Correlation of Side Resistance with Undrained Shear Strength s_u of Soils

For cohesive soils, the side resistances of piles are usually calculated on the basis of the undrained shear strengths of the soils. For the cases investigated in this study, the undrained shear strength of the cohesive soils shown in Table 3 are determined from consolidated isotropic undrained compression (CIUC) tri-axial tests conducted in the laboratory, based on the methods proposed by Leonards (1962).

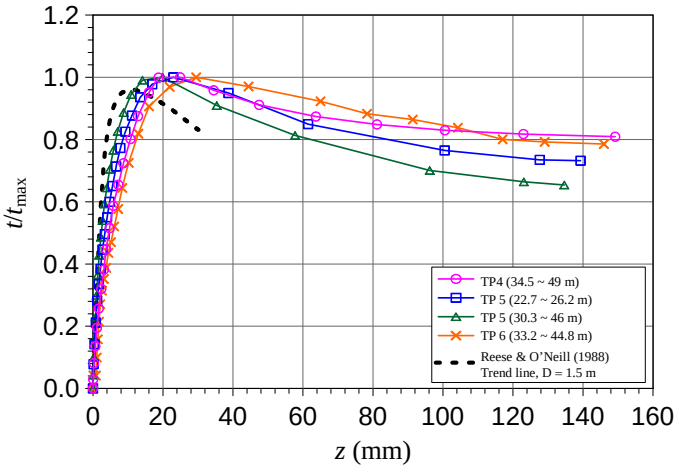

(a) Cohesive soils in Taipei case

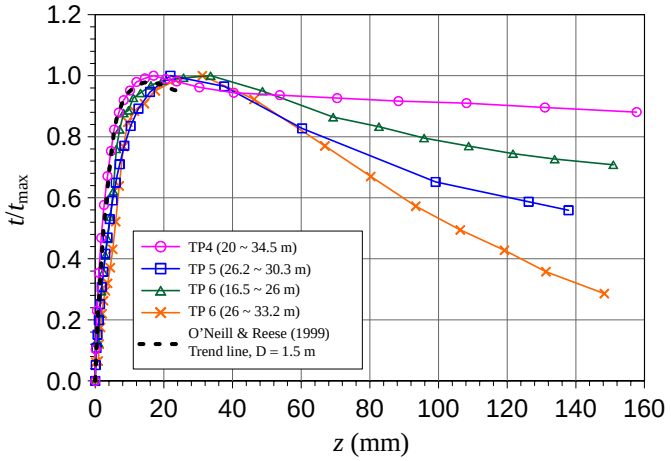

(b) Cohesionless soils in Taipei case

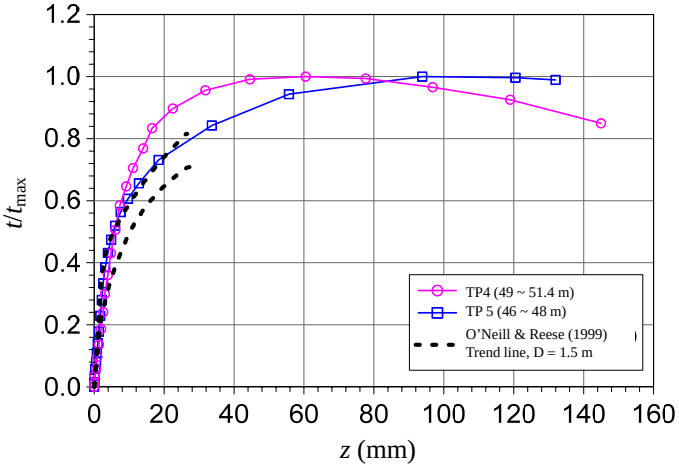

(c) Chingmei gravels in Taipei case

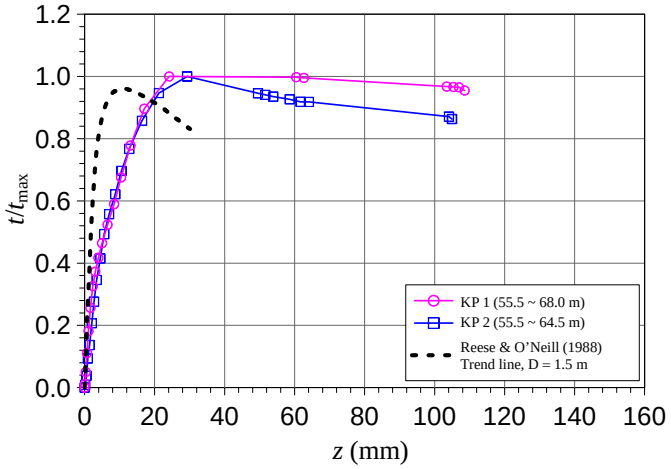

(d) Cohesive soils in Kaohsiung case

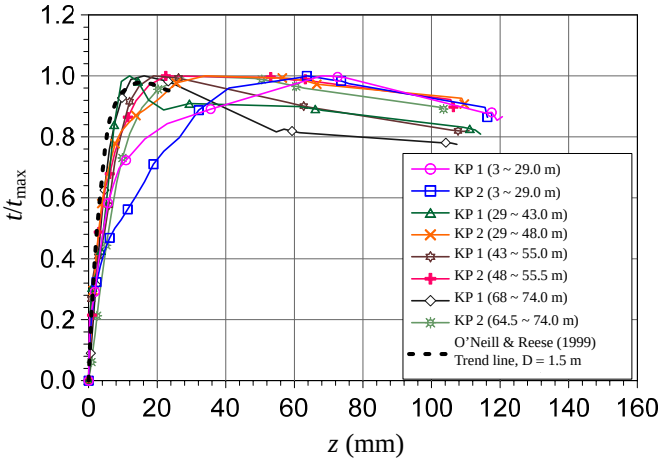

(e) Cohesionless soils in Kaohsiung case

Fig. 15 Normalized *t-z* curves

Table 3 Correlation of side resistance with SPT-*N* value and s_u

Site	Soil Type	Sublayer	Pile No. (depth, m)	$\overline{N}$	s_u (kPa)	$t_{max}/\overline{N}$ (kPa)	$t_{res}/\overline{N}$ (kPa)	t_{max}/s_u	t_{res}/s_u
Taipei	Cohesive	III. CL	TP4 (34.5 ~ 49.0)	11.3	137	10.6	9.0	0.88	0.74
		III. CL	TP5 (30.3 ~ 46.0)	11.6	115	8.0	5.9	0.81	0.60
		III. CL	TP6 (33.2 ~ 44.8)	10.0	129	14.0	12.3	1.09	0.95
		IIB. SM/CL	TP5 (22.7 ~ 26.2)	6.0	84	14.2	11.7	1.01	0.83
	Cohesionless	IIB. SM/CL	TP4 (20.0 ~ 34.5)	16.7	–	4.1	3.8	–	–
		IIB. SM/CL	TP5 (26.2 ~ 30.3)	17.7	–	5.5	4.1	–	–
		IIB. SM/CL	TP6 (16.5 ~ 26.0)	12.5	–	7.8	6.6	–	–
		IIB. SM/CL	TP6 (26.0 ~ 33.2)	13.0	–	6.8	4.5	–	–
	Gravel	IV. GW	TP4 (49.0 ~ 51.4)	> 50	–	–	–	–	–
		IV. GW	TP5 (46.0 ~ 48.0)	> 50	–	–	–	–	–
Kaohsiung	Cohesive	IV. CL	KP1 (55.5 ~ 68.0)	20.0	258	7.6	7.4	0.59	0.57
		IV. CL	KP2 (55.5 ~ 64.5)	10.0	258	11.9	10.4	0.46	0.40
	Cohesionless	I. SM1	KP1 (3.0 ~ 29.0)	13.4	–	3.7	3.4	–	–
		I. SM1	KP2 (3.0 ~ 29.0)	12.6	–	4.9	4.5	–	–
		II. ML/CL	KP1 (29.0 ~ 43.0)	12.2	–	6.7	5.6	–	–
		II. ML/CL	KP2 (29.0 ~ 48.0)	15.5	–	5.5	5.2	–	–
		III. ML	KP1 (43.0 ~ 55.5)	22.7	–	4.1	3.4	–	–
		III. ML	KP2 (48.0 ~ 55.5)	28.0	–	3.1	2.9	–	–
		V. SM2	KP1 (68.0 ~ 74.0)	32.5	–	5.3	4.2	–	–
		V. SM2	KP2 (64.5 ~ 74.0)	46.0	–	4.0	3.7	–	–

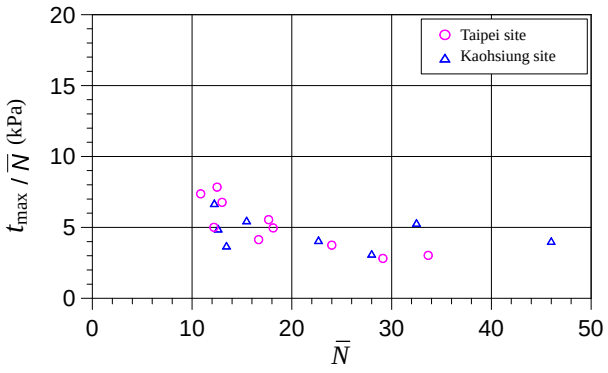

(a) $t_{max}/\overline{N}$ *vs.* $\overline{N}$

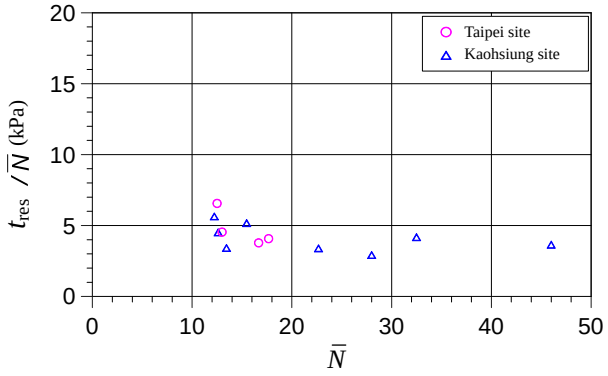

(b) $t_{res}/\overline{N}$ *vs.* $\overline{N}$

Fig. 16 Correlation of side resistance with SPT-*N* value for cohesionless soil

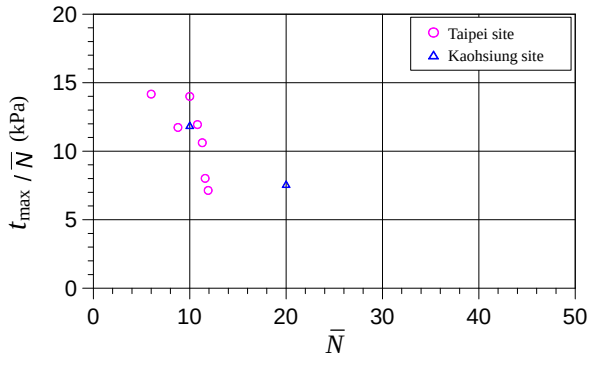

(a) $t_{max}/\overline{N}$ *vs.* $\overline{N}$

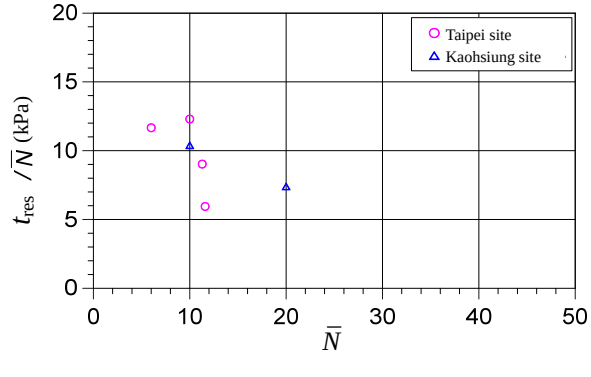

(b) $t_{res}/\overline{N}$ *vs.* $\overline{N}$

Fig. 17 Correlation of side resistance with SPT-*N* value for cohesive soil

For the Taipei and Kaohsiung cases, α_{CIUC}, which defined as t_{max}/s_u and t_{res}/s_u, are calculated as shown in Table 3 and plotted in Figs. 18(a) and 18(b), respectively. It can be seen that the α values for the Taipei clayey soils are larger than those of the Kaohsiung case: The former range from 0.81 ~ 1.09 for the peak side resistance and from 0.60 ~ 0.95 for the residual side resistance, while the latter range from 0.37 ~ 0.47 for the peak side resistance and from 0.32 ~ 0.46 for the residual side resistance. The results obtained in this study are also compared with the results of Chen and Kulhawy (1994, 2003), as shown in Figs. 18(a) and 18(b). The peak resistances are considerably larger than the regression curve in the literature. Even the residual resistances are larger than the regression curve. The regression curve may be considered too conservative to be used to estimate the side resistance of cohesive soils in Taiwan. However, the data obtained in this study are very few, and it can be regarded as a case study only. Hence, further test data are indeed necessary to determine the correlations for practical use in engineering applications.

7. DISCUSSIONS

Based on Fig. 7(d), we can investigate the side resistance of the Chingmei gravel layer in the Taipei area. The *t-z* curves for the gravel formation (Sublayer IV) of TP4 and TP5 exhibit a slight deflection-hardening behavior and have similar ultimate unit side resistances of 550 ~ 600 kPa (Fig. 7(d)). In these cases, the ultimate unit side resistances for the gravel formation are considerably larger than those obtained from load tests of conventional circular large-diameter bored piles in the Taipei area, around 150 ~ 300 kPa (Liao 2008; Wang 2007). In addition, the design value for this layer is only 150 kPa, as estimated on the basis of the empirical formula 3.3*N* kPa by choosing $N = 50$. The main reasons for this discrepancy are discussed below.

Figures 19 and 20 show the profiles measured from ultrasonic echo-sounding tests for the trenches excavated for piles TP4 and TP5. The profiles appear to indicate enlargement of the trench thickness and significant surface irregularities from a depth of 1 ~ 2 m above the surface level of the gravel layer down to the pile toe, especially for the part within the gravel formation. Such surface irregularities in gravel formations, which might be caused by trenching with a bucket or by a localized collapse of the trench surface, are more common with barrette piles than circular piles. This irregularity or roughness of the surface is thought to be the main cause of the significant increase in side resistance from the pile length socked in a gravel formation.

The formation of significant trench wall irregularities in the gravel layer is inevitable when using a MASAGO hydraulic long bucket. Its extent, which is generally associated with the particle size distribution and consistency of soil, as well as the construction technique applied, is difficult to be evaluated prior to construction. Typical particle size distribution curves and an image of the gravel composition for the Taipei site are shown in Fig. 21. The content of gravel and cobbles is around 70%, with a maximum grain size greater than 300 mm.

The Joint Roughness Coefficient (*JRC*) defined by Barton (1973) is temporarily employed to quantify the surface irregularities of a barrette pile in order to investigate the increased side resistance from pile length socked in a gravel formation. The *JRC* at the pile-soil interface in the gravel formation was estimated to be 10 ~ 20 (Figs. 19 and 20). As a preliminary measure based on Barton's study (1973) of the surface roughness of rock joints, the increase in side resistance in gravel formations derived from wall roughness can be roughly estimated to be between 50% and 100%. This contribution to the significant increase in side resistance in gravel formations is larger for a barrette pile than for a circular drilled shaft, owing to the wall roughness caused by the use of a MASAGO hydraulic long bucket.

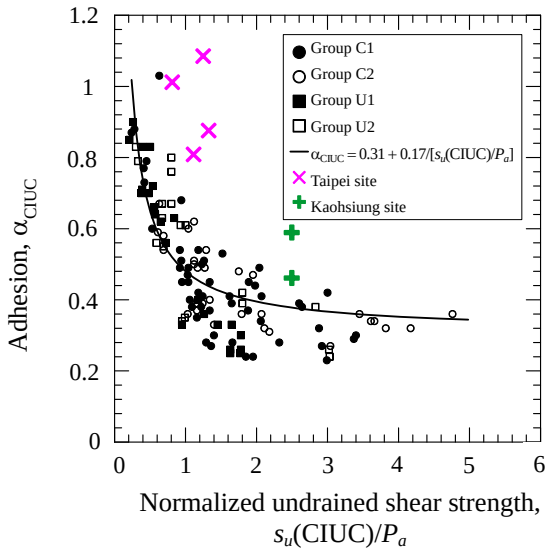

(a) Maximum side resistance

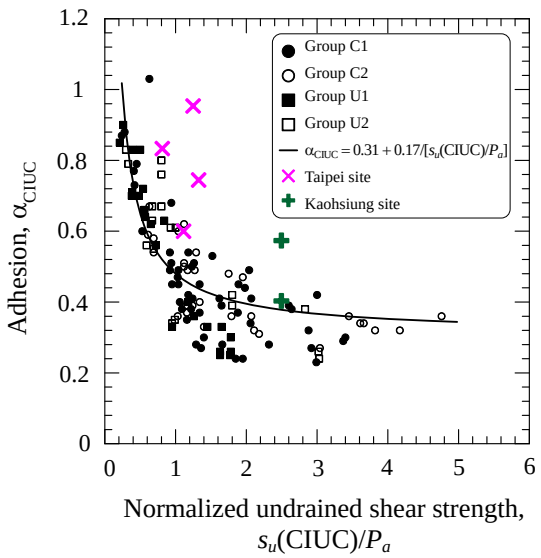

(b) Residual side resistance

Fig. 18 Correlation of α_{CIUC} and $s_{u(CIUC)}/P_a$ (Modified from Chen and Kulhawy 1994, 2003)

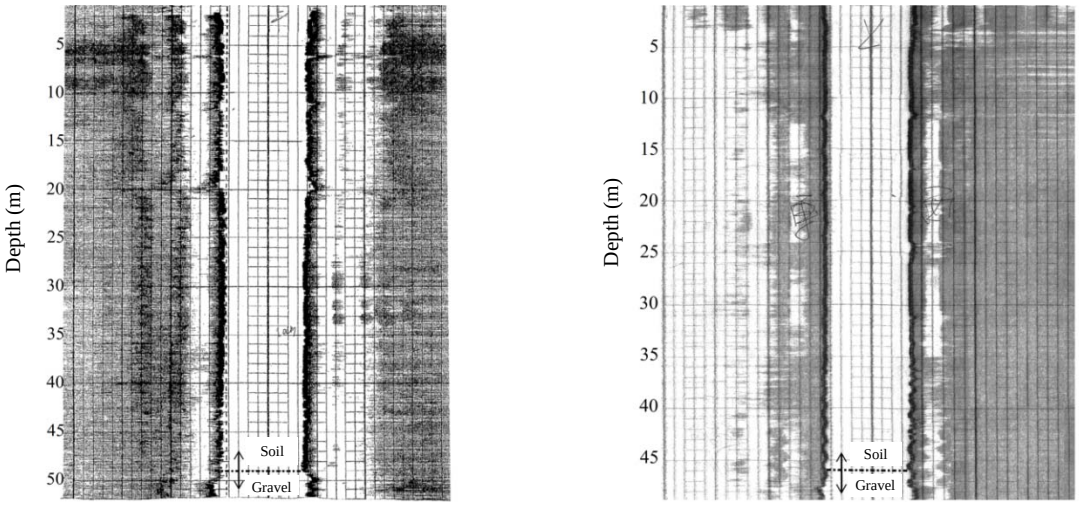

(a) TP4 pile (b) TP5 pile

Fig. 19 Excavation profiles from ultrasonic echo-sounding test

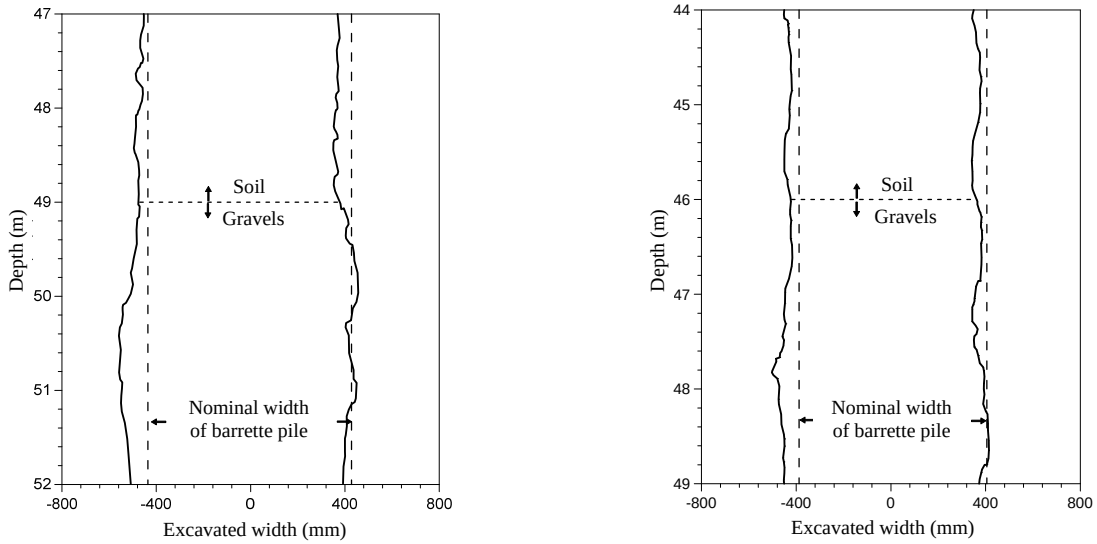

(a) TP4 pile (b) TP5 pile

Fig. 20 Enlarged excavation profiles near the pile toe

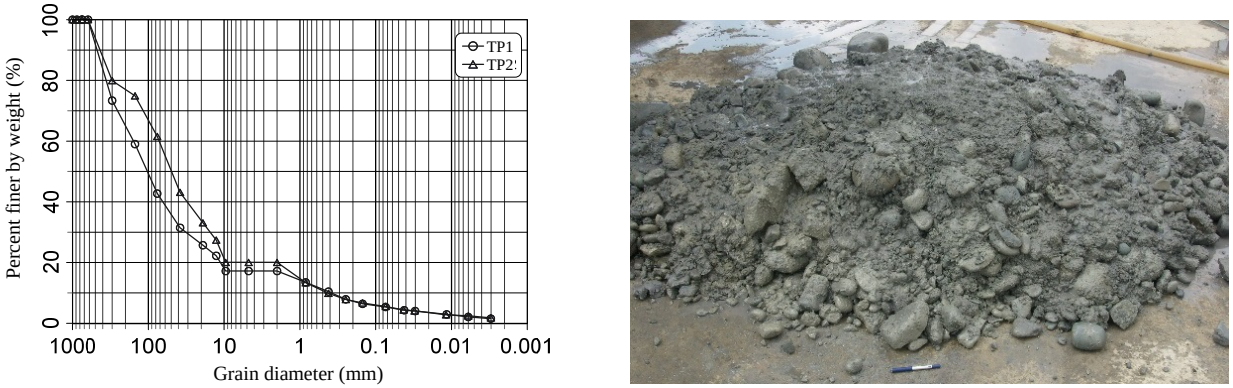

(a) Particle size distribution curves (b) Image of a typical sample of the gravel formation material

Fig. 21 Typical particle size distribution of gravel formation from the Taipei site

8. CONCLUSIONS

Based on the studies conducted herein, the following general conclusions can be drawn:

1. Complete *t-z* curves of soils for the cases of Taipei and Kaohsiung were retrieved from load tests of five barrette piles that were loaded to their ultimate conditions. The characteristics of side resistance for *in situ* barrette piles can thus be investigated.
2. The *t-z* curves for both cohesive and cohesionless soils in the cases investigated indicate a deflection-softening behavior. The peak side resistances were mobilized at a local pile displacement of approximately 20 mm. The ratios of the residual side resistance to maximum side resistance were distributed in the range 0.79 ~ 0.92.
3. Compared with the field test results, the empirical formula 3.3*N* kPa specified in the Design Specifications of Structural Foundations of Taiwan is rather too conservative to be used to estimate the peak side resistance of cohesionless soils on barrette piles, while it is appropriate for estimating the residual side resistance on barrette piles.
4. The case studies conducted in this study show that the empirical αs_u method, specified in the Design Specifications of Structural Foundations of Taiwan, may be too conservative to be used to estimate the peak and residual side resistances of cohesive soils on barrette piles.
5. The *t-z* curves of the Taipei Chingmei gravel obtained in this study exhibited a deflection-hardening behavior. The side resistances determined are much larger than the design values conventionally adopted. One of the reasons for this may be due to the irregularities on the surfaces of the barrette piles, since they are constructed using a hydraulic bucket.

REFERENCES

API (American Petroleum Institute) (2000). *Recommended Practice for Planning, Designing and Constructing Fixed Offshore Platform-Working Stress Design*. API Recommended Practice 2A-WSD, 21th Edition, 55–63.

ASTM (American Society of Testing and Materials) (2007). *Designation: D1143/D1143M-07: Standard Test Methods for Deep Foundations Under Static Axial Compressive Load*.

Barton, N.R. (1973). "Review of a new shear strength criterion for rock joints." *Engineering Geology*, **7**, 287–332.

Chang, Y.H., Hsieh, J.T., Ro, T.R., and Shih, C.H. (2011). "Construction and load testing of barrette foundations." *Sino-Geotechnics*, **128**, 47–58 (in Chinese).

Chen, Y.J. and Kulhawy, F. (2003). "Evaluation of undrained side and tip resistances for drilled shafts." *Soil and Rock America*, **2**, 1963–1968.

Chen, Y.J. and Kulhawy, F. (1994). *Case History Evaluation of Behavior of Drilled Shafts Under Axial and Lateral Loading*, Report TR-104601, EPRI, Palo Alto.

Coyle, H.M. and Reese, L.C. (1966). "Load transfer for axially loaded piles in clay." *Journal of the Soil Mechanics and Foundations Division*, **9**(6), 1–26.

Ho, C.E. and Lim, C.H. (1998). "Barrettes designed as friction foundations: A case history." *Proceedings of the 4th International Conference on Case Histories in Geotechnical Engineering*, St. Louis, Missouri, 236–241.

JRA (Japan Road Associations) (2012). *Specifications for Highway Bridges-No. 5, Substructure*. Tokyo (in Japanese).

Leonards, G.A. (1962). *Foundation Engineering*. McGraw-Hill, New York, 208–217.

Liao, H.C. (2008). *Performance Analysis of Reversed Circulation Pile in Eastern Taipei Area*. M.Sc. Thesis, National Taiwan University of Science and Technology, Taipei, Taiwan (in Chinese).

MOI (Construction and Planning Agency, Ministry of Interior) (2001). *Design Specification for Structural Foundations*, Ch5, Taipei (in Chinese).

Ng, C.W.W. and Lei, G.H. (2003). "Performance of long rectangular barrettes in granitic saprolites." *Journal of Geotechnical and Geoenvironmental Engineering*, **129**(8), 685–696. doi: 10.1061/(ASCE)1090-0241(2003)129:8(685).

Ng, C.W.W., Rigby, D.B., Ng, S.W.L., and Lei, G.H. (2000). "Field studies of well-instrumented barrette in Hong Kong." *Journal of Geotechnical and Geoenvironmental Engineering*, **126**(1), 60–73. doi: http://dx.doi.org/10.1061/(ASCE)1090-0241(2000)126:1(60).

O'Neill, M.W. and Reese, L.C. (1999). *Drilled Shafts: Construction Procedures and Design Methods*. Publication No. FHWA-IF-99-025, Federal Highway Administration, USA.

Reese, L.C., Isenhower, W.M., and Wang, S.T. (2006). *Analysis and Design of Shallow and Deep Foundations*. John Wiley & Sons, Hoboken, New Jersey, Ch13, 413–440.

Reese, L.C. and O'Neill, M.W. (1988). "Field load test of drilled shaft." *Proceedings of International Seminar on Deep Foundations on Bored and Auger Piles*, Van Impe (ed.), Balkema, Rotterdam, 145–192.

RTRI (Railway Technical Research Institute) (1997). *Design Standards for Railway Structures and Commentary - Foundation Structure, Earth Structures*. Tokyo (in Japanese).

Tsai, Y.C. (2006). *Case Study for Axial Load Test of Wall-Type Piles*, M.Sc. Thesis, National Taiwan University, Taipei, Taiwan (in Chinese).

Wang, K.J. (2007). *Skin Friction of Reverse-Circulation Drilled Shafts in Sinyi Development Zone of Taipei Basin*. M.Sc. Thesis, National Taiwan Ocean University, Keelung, Taiwan (in Chinese).

Yu, C.H. (2015). "Application and development of load tests on cast-in-place bored piles in Taiwan." *Proceedings of the 5th Deep Foundation Engineering Development Forum*, Hangzhou, China, 218–235 (in Chinese).

Yu, C.H., Hsu, M.C., and Chien, C.L. (2013). "Application and case study of barrette piles in Taiwan." *Proceedings of the 2013 Cross-Strait Seminar on Geotechnics*, Taipei, Taiwan. 241–252 (in Chinese).